Soft Matter

RSC Publishing

PAPER

View Article Online
View Journal | View Issue

Cite this: *Soft Matter*, 2013, **9**, 2212

Mechanisms of triple-shape polymeric composites due to dual thermal transitions

Qi Ge,[a] Xiaofan Luo,[bcd] Christian B. Iversen,[bc] Patrick T. Mather,[bc] Martin L. Dunn[a] and H. Jerry Qi*[a]

Received 5th September 2012
Accepted 6th December 2012

DOI: 10.1039/c2sm27063c

www.rsc.org/softmatter

Shape memory polymers (SMPs) are a class of smart materials capable of fixing a temporary shape and recovering the permanent shape in response to environmental stimuli such as heat, electricity, irradiation, moisture, or magnetic field, among others. Recently, multi-shape SMPs, which are capable of fixing more than one temporary shape and recovering sequentially from one temporary shape to another and eventually to the permanent shape, have attracted increasing attention. In general, there are two approaches to achieve a multi-shape memory effect (m-SME): the first one requires the SMP to have a broad temperature range of thermomechanical transition, such as a broad glass transition. The second approach uses multiple transitions to achieve m-SME, most notably, using two distinct transition temperatures to obtain a triple-shape memory effect (t-SME). The recently reported approach for designing and fabricating triple-shape polymeric composites (TSPCs) provides a much larger degree of design flexibility by separately tuning the two functional components (matrix and fiber network) to achieve optimum control of properties. The triple-shape memory behavior demonstrated by a TSPC is studied in this paper. This composite is composed of an epoxy matrix, providing a rubber–glass transition to fix one temporary shape, and an interpenetrating crystallizable PCL fiber network providing the system the melt–crystal transition to fix a second temporary shape. A one-dimension (1D) model that combines viscoelasticity for amorphous shape memory polymers (the matrix) with a constitutive model for crystallizable shape memory polymers (the fiber network) is developed to describe t-SME. The model includes the WLF and Arrhenius equations to describe the glass transition of the matrix, and the kinetics of crystallization and melting of the fiber network. The assumption that the newly formed crystalline phase of the fiber network is initially in a stress-free state is used to model the mechanics of evolving crystallizable phases. Experiments including uniaxial tension, stress relaxation, and triple-shape memory testing were carried out for parameter identification. The model accurately captures t-SME exhibited in experiments. The stress and stored energy analysis during the shape memory cycle provides insight into the mechanisms of shape fixing for the two different temporary shapes, the nature of both recovery events, as well as a guidance on how to design transitions to achieve the desired behavior.

1 Introduction

Shape memory polymers (SMPs) are a class of smart polymers that can fix a temporary shape and recover their permanent shape in response to environmental stimulus such as heat,[1–5] light,[6–14] moisture,[15] and magnetic field,[16] among others. Among the SMPs developed recently, thermally triggered SMPs are the most widely investigated.[17] Compared to shape memory alloys, SMPs are extraordinarily stretchable (up to 1100%),[1] have low density, are inexpensive and easier to fabricate, degradable and tailorable.[1,2] These advantages allow SMPs to be used in many applications such as microsystem actuation components, recoverable surface patterns, biomedical devices, aerospace deployable structures, and morphing structures.[1,2,17–22]

For a thermally triggered SMP, a thermomechanical cycle starts by deforming the material at a temperature T_H above a transition temperature T_{Trans}. The material is then cooled down to a temperature T_L below T_{Trans}, while maintaining the deformed shape. At T_L, the deformed shape is fixed after removal of the external load. This deformed shape is usually termed as the programmed shape or temporary shape. Shape recovery is activated by increasing the temperature to T_H and the material recovers its initial shape or permanent shape under the driving force of rubber elasticity from an underlying

[a]*Department of Mechanical Engineering, University of Colorado, Boulder, CO 80309, USA. E-mail: qih@colorado.edu*

[b]*Syracuse Biomaterials Institute, Syracuse University, Syracuse, NY, 13244, USA*

[c]*Department of Biomedical and Chemical Engineering, Syracuse University, Syracuse, NY, 13244, USA*

[d]*Flow Polymers LLC, 12819 Coit Rd, Cleveland, OH, USA*

network of covalent or physical crosslinks. In this thermomechanical cycle, a SMP has two shapes, namely the temporary shape and the permanent shape. Therefore, it is sometimes referred to as a "dual-shape" SMP. A physical mechanism is required to effect the transition between the two shapes – two examples are the glass transition between the rubbery and the glassy states[23–26] and the transition between crystals and melts.[27–30]

Along with strong interests in dual-shape SMPs, multi-shape SMPs have started to attract increasing attention. To date, there are two approaches to achieve a multi-shape memory effect (m-SME). The first approach requires the SMP to have a wide temperature range of thermomechanical transition. For example, Xie[31] recently demonstrated that perfluorosulphonic acid ionomer (PFSA), a thermo-plastic SMP with a broad glass transition temperature range from 55 °C to 130 °C, could show m-SME, if the temperature is increased during recovery in a staggered manner. Using a simple theoretical model, we found that the physical mechanism of this observed m-SME is due to the multiple relaxation modes of macromolecular chains, these relaxation modes being sensitive to temperature.[32] At a particular temperature during recovery, some relaxation modes are active (meaning their relaxation time is comparable with the lab time scale), while some other relaxation modes are not (meaning their relaxation time is extremely long as compared to the lab time scale). If the temperature is increased in a staggered manner, the number of active relaxation modes also increases in a staggered manner, leading to the observed m-SME.

The second approach is to use multiple transition temperatures to achieve m-SME, most notably, to use two distinct transition temperatures to obtain the triple-shape memory effect (t-SME). Here, t-SME refers to fixing two temporary shapes and recovering sequentially from one temporary shape to the other upon continuous heating, and ultimately to the permanent shape.[33–36] In a typical thermomechanical triple-shape memory cycle (Fig. 1), in Step 1 (S1), the material is initially deformed at a temperature T_H, where T_H is higher than two phase transition temperatures ($T_{Trans\ I}$ and $T_{Trans\ II}$). In Step 2 (S2), the temperature is decreased to T_{L1} ($T_{L1} < T_{Trans\ I}$), while maintaining the external load resulting in the deformation in S1. After removal of the external load, in Step 3 (S3), fixing of the first temporary shape at T_{L1} is revealed. In Step 4 (S4), the sample is deformed further at T_{L1} (*note*: this need not be in the same direction or in the same plane as the first deformation.) In Step 5 (S5), the material is cooled to T_{L2} ($T_{L2} < T_{Trans\ II}$), while keeping the external load causing the deformation in S4. In Step 6 (S6), after unloading, the second temporary shape is fixed at T_{L2}. In Step 7 (S7), as the sample is heated back to T_{L1}, the material recovers into its first temporary shape. In Step 8 (S8), the permanent shape is reached by heating to T_H.

Recently, several methods of achieving the t-SME were reported. Bellin and co-workers[33,34] developed two different polymer networks to achieve the t-SME. These two network systems are macroscopically homogeneous with two microscopic polymer segments. The two phase transitions are either glass transition of one segment and crystal–melt transition of the other one, or two crystal–melt transitions of two different

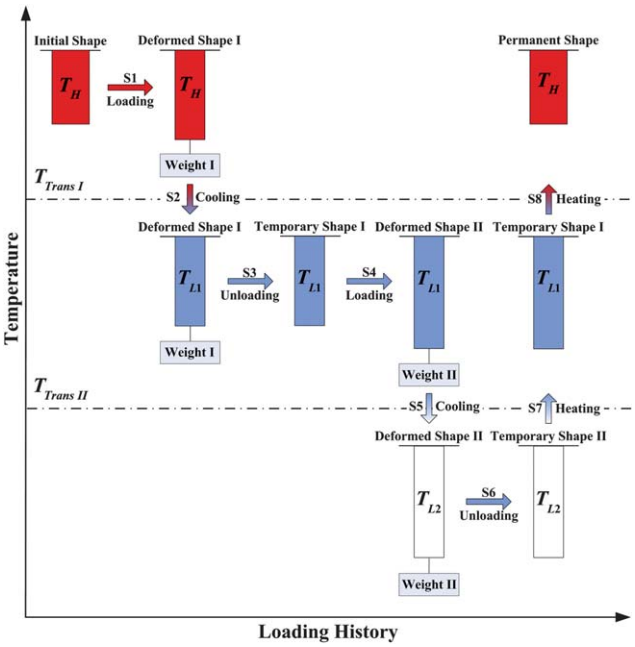

Fig. 1 Schematic of a thermomechanical triple shape memory cycle. At S1, where $T_H > T_{Trans\ I} > T_{Trans\ II}$, the material is initially deformed by Weight I. At S2, the temperature is decreased to T_{L1} ($T_{Trans\ I} > T_{L1} > T_{Trans\ II}$), while maintaining Weight I. At S3, after removal of Weight I at T_{L1}, the first temporary shape is fixed. At S4, the material is further deformed by Weight II at T_{L1}. At S5, the temperature is cooled down to T_{L2} ($T_{L2} < T_{Trans\ II}$), while keeping Weight II. At S6, the fixing of the second temporary shape is revealed by removing Weight II at T_{L2}. At S7, the material recovers into its first temporary shape, as the temperature is heated back to T_{L1}. At S8, the permanent shape is reached by heating to T_H.

segments. Xie *et al.*[36] reported a different method of achieving the t-SME using a macroscopic bilayer crosslinked polymer structure with two well separated phase transitions. Recently, based on the fabrication of shape memory elastomeric composites (SMECs),[27] Luo and Mather[35] introduced a new and broadly applicable method for designing and fabricating triple shape polymeric composites (TSPCs) with well controlled properties. In the TSPC, an amorphous SMP (epoxy with $T_g \approx$ 20–40 °C, depending on the precise composition) works as the matrix providing overall elasticity and provides one phase transition temperature, and non-woven PCL (poly(ε-caprolactone)) microfibers produced by electrospinning and incorporated into the matrix provide the other phase transition temperature due to the crystal–melt transition of PCL ($T_m \approx$ 50 °C). Compared with methods reported previously, the approach for fabricating polymeric composites is quite flexible, since one can tune the functional components separately to optimize material properties, opening up the potential to design for a variety of applications.[35]

Constitutive models were also developed in the past for SMPs. These models were mainly for dual-shape SMPs, including the early model by Tobushi *et al.*,[37] the modified standard linear solid model with the Kohlrausch–Williams–Watts (KWW) stretched exponential function by Castro *et al.*,[38] three dimensional finite deformation models for amorphous SMPs developed by Liu *et al.*,[18] Qi *et al.*,[23] Nguyen *et al.*,[24] Chen and Lagoudas,[39,40] and Westbrook *et al.*;[41] constitutive models

for crystallizable shape memory polymers were developed by Barot and Rao,[42] Westbrook *et al.*,[30] and Ge *et al.* for SMECs.[28] For multi-shape SMPs, Yu *et al.*[32] demonstrated that a multi-branch model can be used to capture the m-SME in SMPs with a broad range of transition temperatures. For the t-SME with dual transition temperatures, to the authors' best knowledge, no model has been reported to date.

This paper investigates the triple-shape memory behavior of TSPC and presents a one-dimension (1D) model to describe the triple-shape memory behavior. In the model, the macroscopic behavior of the composite depends on two phases the composite is made up of. Each phase of the composite can undergo individual phase transition (the glass transition for the matrix and the crystal–melt transition for the fiber network) and contributes to the macroscopic behavior. The model separately considers the glass transition and crystal–melt transition. This separate treatment allows the material parameters used in the model to be independently identified from experiments. The parameter identification approaches are proposed and the necessary tests are described. The paper is arranged in the following manner: in Section 2, the material is introduced briefly and experimental results including DMA, stress relaxation tests, uniaxial tension tests and triple-shape memory behaviors are presented. Section 3 introduces the 1D model. In Section 4, parameter identification is introduced and, with parameters having been determined by experiments, simulations of stress and stored energy analysis for the triple-shape memory behavior are presented.

2 Materials and thermomechanical behaviors

2.1 Materials

A TSPC was prepared using an epoxy-based copolymer thermoset system as the matrix and a poly(ε-caprolactone) (PCL) as fiber reinforcements. For the epoxy-based copolymer thermoset system, it consists of an aromatic diepoxide (diglycidyl ether of bisphenol-A or DGEBA), an aliphatic diepoxide (neopentyl glycol diglycidyl ether or NGDE) and a diamine curing agent (poly(propylene glycol) bis(2-aminopropyl) or Jeffamine D230).[35] In this paper, the mole% ratio DGEBA : NGDE = 30 : 70 or D30N70 was chosen for all tests. The fabrication is similar to that of previously reported shape memory elastomeric composites (SMECs).[27,35]

2.2 DMA experiments

DMA tests were conducted using a dynamic mechanical analyzer (Q800 DMA, TA Instruments). The epoxy/PCL TSPC (a 11.65 mm × 1.7 mm × 0.43 mm rectangular film) was stretched by a dynamic tensile load at 1 Hz. The temperature was first cooled at a rate of 1 °C min^{-1} from 100 °C to −50 °C, then after 10 min thermal equilibration at −50 °C, it was heated up to 100 °C at a rate of 1 °C min^{-1}. Fig. 2 shows the tensile storage modulus with temperature. The heating trace and the cooling trace show different features. In the heating trace, it clearly shows two separated thermal transitions, corresponding to the glass–rubber transition of epoxy and the crystal–melt transition of PCL, respectively. As a result, a cascade of three storage modulus plateaus of decreasing magnitude with increasing temperature was observed. The first high modulus plateau (~1.5 GPa) exists below epoxy T_g^{epoxy} attributed to the glassy state of epoxy (Plateau I in Fig. 2). The second moderate modulus plateau (~10 MPa) lies between epoxy T_g^{epoxy} and PCL T_m^{PCL}, where epoxy is in the rubbery state but PCL is in the semi-crystalline state (Plateau II in Fig. 2). Above PCL T_m^{PCL}, there is a low modulus plateau (~2 MPa) (Plateau III, in Fig. 3). Different from the heating trace, during cooling, the rubber–glass transition of epoxy and the melt–crystal transition of PCL are largely merged into one single transition and Plateau II disappears. This is primarily attributed to two close temperature ranges of two transitions, and the supercooling that is inherent to

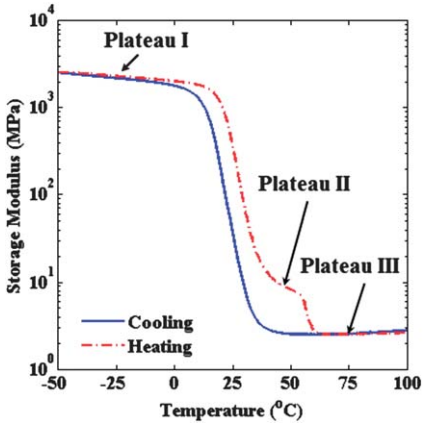

Fig. 2 DMA results for the epoxy/PCL TSPC: storage modulus with temperature during a cooling–heating cycle. During heating, a cascade of three storage modulus plateaus was observed. At Plateau I, the matrix (epoxy) is in the glassy state and the fiber network (PCL) is in the semicrystalline state. At Plateau II, the matrix is in the rubbery state, but the fiber network is still in the semicrystalline state. At Plateau III, the matrix is in the rubbery state and the fiber network is in the melting state. During cooling, Plateau II disappears.

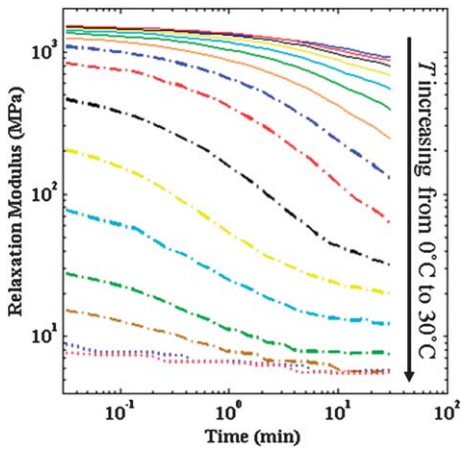

Fig. 3 Tensile relaxation modulus for temperatures varying from 0 °C (indicate color or insert line) to 30 °C (indicate color or insert line) with 2 °C temperature intervals between experiments.

polymer crystallization. A significant hysteresis between the heating and the cooling traces are observed, especially between the melting at ~55 °C and the crystallization at ~30 °C. The major reason resulting in the significant hysteresis is due to the difference between the kinetics of crystallization and melting. For example, crystallization occurs only at temperatures below the crystallization temperature whilst melting only occurs at temperatures above the melting temperature. For polymers, the crystallization and melting temperatures are identical or very close to each other.

2.3 Stress relaxation tests

Stress relaxation tests were conducted using the DMA machine in order to yield the viscoelastic data required by material parameter estimations needed for our modeling. A rectangular TSPC sheet with the dimension of 8.97 mm × 1.71 mm × 0.43 mm was used for tests. Stress relaxation tests were performed at 16 different temperatures evenly distributed from 0 °C to 30 °C, a temperature safely below the melting point of the fiber network. The sample was preloaded by application of a small, 1×10^{-3} N force to maintain its straightness. After reaching the testing temperature, it was thermally equilibrated for 30 min. Then a 0.1% strain was applied to the sample and the relaxation modulus was observed for 30 min. Fig. 3 shows the results of stress relaxation for 16 different temperatures. Based on the well-known time temperature superposition principle (TTSP),[43,44] a relaxation master curve was achieved by shifting relaxation curves to a reference temperature of T_r = 16 °C, with temperature-dependent shifting factors. The relaxation master curve and shifting factors will be reported in Section 4.

2.4 Uniaxial tension tests

The uniaxial tension tests for both the neat epoxy and the TSPC were conducted using the DMA machine. The dimensions of the neat epoxy sample and the TSPC sample were 9.09 mm × 1.8 mm × 1.44 mm and 9.97 mm × 1.97 mm × 0.5 mm, respectively. Both samples were tested at 40 °C and 80 °C respectively, at the loading rate of 0.5 MPa min^{-1}. The results of uniaxial tensions were used for parameter identification, which will be introduced in Section 4.1.

2.5 Shape memory behavior

Shape memory behaviors were tested on the DMA machine with a 10.69 mm × 2.25 mm × 0.42 mm rectangular film. The t-SME was achieved by following an eight-step-shape-fixing method proposed by Luo and Mather:[35] in Step 1 (S1), the material is initially stretched at a stress rate of 0.5 MPa min^{-1} to a constant load P_1 at a temperature T_H ($T_H > T_g^{epoxy}, T_m^{PCL}$). In Step 2 (S2), the material is cooled down at a rate of 2 °C min^{-1} to a temperature T_{L2} ($T_{L2} < T_g^{epoxy}, T_m^{PCL}$) while maintaining the load P_1. In Step 3 (S3), it is heated up at a rate of 2 °C min^{-1} to a temperature T_{L1} ($T_g^{epoxy} < T_{L1} < T_m^{PCL}$). In Step 4 (S4), after unloading, the first temporary shape is fixed at T_{L1}. In Step 5 (S5), the material is stretched at the same stress rate of S1 to a constant load P_2 ($P_2 > P_1$) and the material is in a new deformation state. In Step 6 (S6), it is cooled down to T_{L2} again, while keeping the constant load P_2. In Step 7 (S7), after unloading, the material achieves the second temporary shape at T_{L2}. Finally, in Step 8 (S8), the material is heated up to T_{L1} and it recovers to its first temporary shape and permanent shape sequentially. In this paper, this approach is used where T_H is 80 °C, T_{L1} is 40 °C and T_{L2} is 0 °C. It is emphasized that the cooling to T_{L2} in S2 and the heating to T_{L1} in S3 are necessary to distinguish the two separated phase transitions: in S2, epoxy is in the glassy state and PCL is in the semicrystalline state and in S3, PCL is still in the semicrystalline state but epoxy is in the rubbery state. The strain–temperature plots are shown in Section 4 with three different nominal stress pairs (P_1 = 0.1 MPa, P_2 = 0.3 MPa; P_1 = 0.15 MPa, P_2 = 0.45 MPa; P_1 = 0.2 MPa, P_2 = 0.6 MPa).

As reported by Luo and Mather,[35] the triple-shape behavior can be achieved by a so-called "one-step-fixing" method. In order to better understand the mechanism on how to achieve two temporary shapes after a single fixing step, the material was tested by the "one-step-fixing" method. The material was stretched at a rate of 0.5 MPa min^{-1} to 0.2 MPa at 80 °C and then cooled down to 0 °C at a rate of 2 °C min^{-1}, while maintaining the load; after quickly unloading at 0 °C, almost 100% strain was fixed. During heating, it is quite interesting that there is a strain plateau at ~40 to 60 °C, and at 80 °C, the material was able to completely recover to its permanent shape. In Section 4, we will show that three shapes can be observed: one at 0 °C, one at between 40 °C and 60 °C, and finally one at 80 °C.

3 Model description

3.1 Overall model

In this section, a one dimensional (1D) model is developed to capture the t-SME in the epoxy/PCL TSPCs and to clearly understand the mechanism of shape fixing, stress and strain energy distribution during a shape memory cycle. In this model, the matrix and the fiber network are treated as a homogenized system. The macroscopic behavior of the system depends on the two phases (the matrix and the fiber network). The matrix as an amorphous SMP undergoes the glass transition and the fiber network as the crystallizable polymer undergoes the crystal–melt transition. The fiber network is a liquid (melt) at high temperatures and an elastic solid at low temperature, where melts and crystals co-exist and their respective volume fractions depend on the temperature and their evolutions are described by the existing theory of crystallization. As the model is primarily focusing on the shape fixing mechanism, we do not seek a rigorous micromechanical description. In addition, the thermal expansion is not introduced for this 1D model, although it can be easily included.[28]

For the TSPC system, the simplest model arranges stresses on the matrix and the fiber network in parallel (as shown in Fig. 4) and the total Cauchy stress σ^{total} is given by:

$$\sigma^{total} = v_M \sigma^M + v_F \sigma^F, \quad (1a)$$

where σ^M and σ^F are the stresses acting on the matrix and the fiber network, v_M and v_F are the volume fractions of the matrix

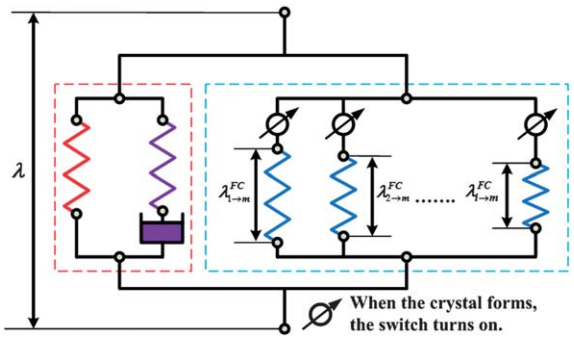

Fig. 4 Schematic of the overall model: the total Cauchy stress consists of stresses on the matrix (red dashed box, left) and stress on the fiber network (blue dashed box, right). For the stress on the matrix, a modified Standard Linear Solid (SLS) model is adopted to consider the equilibrium and nonequilibrium behaviors of the matrix. The multiple springs of the fiber network model represent fiber crystals formed at different times. During crystallization, once a small piece of crystalline phase forms, the corresponding switch turns on. The crystalline phases forming at different times may have different deformation history. During melting, the crystalline phases vanish gradually. Once a small piece of crystalline phase vanishes, the corresponding switch turns off and it does not carry load any more.

and the fiber network, which are determined by fabrication and $v_M + v_F = 1$.

In reality, the stress distribution in the phases depends on details of the microstructure, including the geometry, and architecture of the spatial arrangement of the phases, and the evolution of their properties. We attempt to account for the departure of stress distribution among the phases by borrowing the concept of a stress concentration factor from the micromechanics of heterogeneous solids in linear and nonlinear elasticity.[45–47] Introducing stress concentration factors for the matrix and the fiber network, the total Cauchy stress σ^{total} is written as:

$$\sigma^{total} = \gamma_M v_M \sigma^M + \gamma_F v_F \sigma^F, \quad (1b)$$

where γ_M and γ_F are stress concentration factors of the matrix and the fiber network and $\gamma_M v_M + \gamma_F v_F = 1$.

Fig. 4 shows a rheological representation of the model. The left red dashed box represents the stress acting on the matrix. A modified Standard Linear Solid (SLS) model is adopted to consider both equilibrium and nonequilibrium behaviors of the matrix. Here, a spring is used to represent the equilibrium behavior and a KWW (Kohlrausch, Williams and Watts) stretched exponential function for stress relaxation is used to represent the nonequilibrium viscoelastic response.[48] The right blue dashed box represents the mechanical elements for the fiber network behavior. During crystallization, fiber crystals gradually form. Once a small piece of crystalline phase forms, the corresponding switch in Fig. 4 turns on. Depending on the thermomechanical conditions, the crystalline phases forming at different times may have different deformation history. During melting, the crystalline phases vanish gradually. According to the kinetic description of the melting process, the piece of crystalline phase that grows at a later time melts first.[28] Once a small piece of crystalline phase vanishes, the corresponding switch in Fig. 4 turns off and it does not carry load any more.

3.2 Viscoelastic behavior of the matrix

For the matrix, the modified SLS model is used to consider both equilibrium and nonequilibrium viscoelastic behaviors. The total stress on the matrix consists of contributions from both equilibrium and nonequilibrium behaviors:

$$\sigma^M(T,t) = \sigma^{eq}(T) + \sigma^{non}(T,t). \quad (2)$$

The Cauchy stress from the equilibrium response $\sigma^{eq}(T)$ follows the neo-Hookean model with entropic elasticity:

$$\sigma^{eq}(T) = NkT(\lambda^2 - 1/\lambda), \quad (3)$$

where N is the crosslink density of the matrix, k is Boltzmann's constant, T is the absolute temperature and λ is the stretch along the uniaxial load. $\lambda = 1 + \varepsilon$ and ε is the strain. For the nonequilibrium response, the stress should be:

$$\sigma^{non}(t) = E_{non}\varepsilon_e(t), \quad (4)$$

where E_{non} is the Young's Modulus and ε_e is the elastic strain of the nonequilibrium branch. Using the KWW stretched exponential and Boltzmann superposition principle, ε_e can be:[25]

$$\varepsilon_e(t) = \int_0^t \frac{\partial \varepsilon}{\partial s} \exp\left[-\left(\int_s^t \frac{dt'}{\tau(T,t')} \right)^{\beta} \right] ds, \quad (5)$$

where ε is the total strain in the nonequilibrium $\varepsilon = \varepsilon_e + \varepsilon_v$, ε_v is the viscous strain, $\tau(T)$ is the temperature dependent stress relaxation time. β is a material parameter within a range between 0 and 1 characterizing the width of the stress relaxation distribution, *i.e.* a decrease of β leads to an increase of the stress relaxation breadth. Once β reaches 1, it is the narrowest stress relaxation time distribution and the nonequilibrium branch is reduced to the original Maxwell model. The temperature dependent stress relaxation time $\tau(T)$ is obtained using a shifting factor a_T:

$$\tau(T) = a_T \tau_0, \quad (6)$$

where τ_0 is the stress relaxation time at a reference temperature. It was found that depending on whether the temperature is above and near or below T_g, the shifting factor a_T can be calculated by two different methods.[49] For temperatures above and near T_g, the WLF (Williams–Landel–Ferry) equation[50] is used:

$$\log a_T = -\frac{C_1(T - T_r)}{C_2 + (T - T_r)}, \quad (7)$$

where C_1 and C_2 are material constants, and T_r is a reference temperature. For temperatures below T_g, an Arrhenius-type behavior developed by Di Marzio and Yang (1997)[51] is used:

$$\ln a_T = -\frac{AF_C}{k}\left(\frac{1}{T} - \frac{1}{T_r}\right), \quad (8)$$

where A is the material constant, F_c is the configuration energy and k is Boltzmann's constant.

3.3 Mechanical behavior of the fiber network

For the semicrystalline fiber network, crystallization and melting are functions of temperature and time. We adopt the postulation that when a small fraction of polymer crystals forms, it is in a stress-free state.[29,30] However, in order to satisfy the boundary conditions, either overall or locally, this small fraction will deform immediately. This stress-free state for the newly formed crystalline phases was referred to as the natural configuration by Rajagopal and Srinivasa,[52,53] and has been used by many researchers to study crystallizing polymers,[54–57] rubbers with thermally induced scissoring and reformation,[58–61] shape memory polymers,[42,62,63] and light induced activated polymers.[13] Following this assumption, the stress in the fiber networks is:[29]

$$\sigma^{\mathrm{F}} = \int_{t_c}^{t} \dot{v}(s)\sigma^{\mathrm{FC}}\left[\lambda^{\mathrm{FC}}(t-s)\right]\mathrm{d}s, \tag{9}$$

where t_c is the time point when crystallization starts, $\lambda^{\mathrm{FC}}(t-s)$ is the stretch of the fiber crystals formed at $t = s$ and $v(s)$ is the crystallinity of crystalline phases, which is a function of time and temperature and is discussed below; σ^{FC} is the stress function for fiber crystals. For the sake of simplicity, it is simply assumed that the stress on fiber crystals follows neo-Hookean behavior and the Cauchy stress is:

$$\sigma^{\mathrm{FC}} = \mu_{\mathrm{C}}(\lambda^2 - 1/\lambda), \tag{10}$$

where μ_{C} is the shear modulus of fiber crystals. The incremental description for stress on the fiber network during crystallization and melting was reported.[28]

To describe crystallization kinetics,[64–66] a simplified Avrami's phase transition theory is used. In polymer crystallization, the time–temperature dependent crystallinity of the polymer, $v(T,t)$, can be expressed as:[28]

$$v(T,t) = H_\infty\{1 - \exp[-V(T,t)]\}, \tag{11}$$

where H_∞ is the saturated crystallinity of a polymer under a certain condition; for PCL network H_∞ is taken as 25%[28] and $V(T,t)$ is the volume fraction of crystalline phases without impingement. The calculation of $V(T,t)$ during crystallization or melting was discussed in Ge *et al.*[28]

3.4 Strain energies

Strain energies on the matrix and the fiber network were used to investigate the shape fixing mechanism. For the equilibrium branch of the matrix and individual fiber crystals, as both of them adopt the neo-Hookean constitution, the strain energy on the equilibrium branch of the matrix and individual fiber crystals is:

$$W = \pm\mu(I_1 - 3), \tag{12}$$

where μ is the shear modulus and equal to NkT for the matrix and equal to μ_{C} for fiber crystals; I_1 is the first deformation invariant, for the uniaxial loading case, $I_1 = \lambda^2 + 2/\lambda$. The "±" sign is used to distinguish tensile (+) or compressive (−) loading. For the strain energy of the fiber crystals, it follows:

$$W^{\mathrm{F}} = \int_{t_c}^{t} \dot{v}(s)\,W(t-s)\mathrm{d}s. \tag{13}$$

For the nonequilibrium branch of the matrix, the strain energy is given as follows:

$$W = \pm\frac{1}{2}E_{\mathrm{non}}{\varepsilon_{\mathrm{e}}}^2, \tag{14}$$

where E_{non} is the Young's Modulus and ε_{e} is the elastic strain of the nonequilibrium branch introduced in eqn (5).

4 Results

4.1 Parameter identification

In the model, there are 13 parameters in total (see Table 1). Except the volume fractions which are determined by fabrication ($v_{\mathrm{M}} = 0.82$ and $v_{\mathrm{F}} = 0.18$), rest of them were determined by uniaxial tension and stress relaxation experiments. Specifically, uniaxial tension tests were used to determine the crosslinking density N of the matrix (epoxy), shear modulus of fiber crystals (PCL), and stress concentration factors γ_{M} and γ_{F}. Stress relaxation tests were used to identify the relaxation time τ_0 at 16 °C, KWW stretching parameter β, the Young's modulus for nonequilibrium branch E_{non}, and constants in WLF equation and Arrhenius behavior.

Fig. 5 shows the results from uniaxial tensile experiments of both the neat epoxy and TSPC at 80 °C (Fig. 5a) and at 40 °C (Fig. 5b). By fitting the experimental curve for the neat epoxy at 80 °C, the crosslinking density N was identified as 3.84×10^{-23} m^{-3}. For the TSPC at 80 °C, as the fiber network melts, $\sigma^{\mathrm{F}} = 0$. Therefore, the total stress is:

$$\sigma^{\mathrm{total}} = \gamma_{\mathrm{M}}v_{\mathrm{M}}NkT(\lambda^2 - 1/\lambda). \tag{15}$$

By fitting the TSPC curve at 80 °C (Fig. 5a), we obtained $\gamma_{\mathrm{M}} = 0.57$ and $\gamma_{\mathrm{F}} = 2.94$. For the TSPC at 40 °C, as the crystallization of PCL finishes before the test, the Cauchy stress follows:

$$\sigma^{\mathrm{total}} = \gamma_{\mathrm{M}}v_{\mathrm{M}}NkT(\lambda^2 - 1/\lambda) + \gamma_{\mathrm{F}}v_{\mathrm{F}}H_\infty\mu_{\mathrm{C}}(\lambda^2 - 1/\lambda). \tag{16}$$

In eqn (16), only the shear modulus μ_{C} for PCL crystals is unknown and can be determined easily by fitting the uniaxial tension for TSPC at 40 °C. Fig. 5b shows the fitting result with $\mu_{\mathrm{C}} = 9.2$ MPa.

Based on the time–temperature superposition principle, a relaxation master curve at 16 °C (Fig. 6a) can be achieved by shifting individual relaxation curves with shifting factors at different temperatures.[43,44] The relaxation master curve can be described by a modified standard linear solid model with the KWW stretch exponential, where the stress relaxation modulus should be:

$$E(t) = E_0 + E_1\exp\left[-\left(\frac{t}{\tau_0}\right)^{\beta}\right]. \tag{17}$$

In eqn (17), at time $t = 0$, $E(0) = E_0 + E_1$ and when t approaches ∞, $E(\infty) = E_0$. From Fig. 6a, we have $E_0 = 8$ MPa

Table 1 List of material parameters

Parameters	Value	Description
Composition		
ν_M	0.82	Volume fraction of the matrix (epoxy)
ν_F	0.18	Volume fraction of the fiber network (PCL)
γ_M	0.57	Stress concentration factor of the matrix (epoxy)
γ_F	2.94	Stress concentration factor of the fiber network (PCL)
Epoxy matrix		
N	3.84×10^{-23} m^{-3}	Polymer crosslinking density
E_{non}	3150 MPa	Young's modulus for the nonequilibrium branch
τ_0	110 s	Relaxation time at 0 °C
β	0.3	KWW stretching parameter
T_r	16 °C	Reference temperature
C_1	24	WLF constant
C_2	50 °C	WLF constant
AF/k	−35 000 K	Pre-exponential parameter for Arrhenius-type behavior
PCL fiber network		
μ_C	9.2 MPa	Shear modulus for PCL crystals

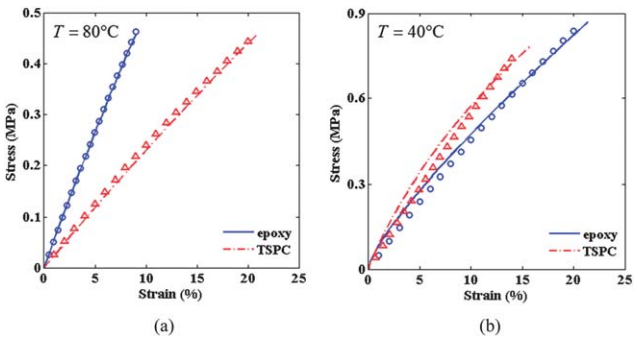

Fig. 5 Model fitting for uniaxial loadings. (a) At 80 °C and (b) at 40 °C. (Blue circles represent the model fitting for the neat epoxy; red triangles represent the model fitting for the TSPC.)

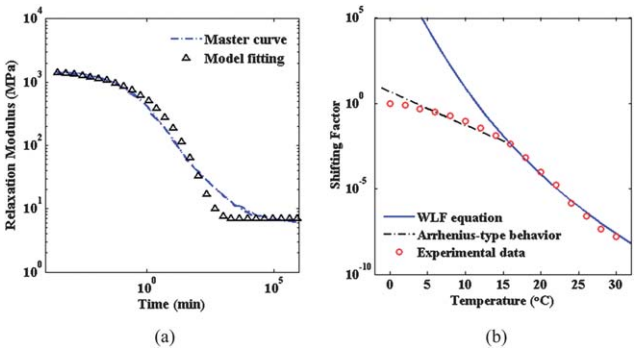

Fig. 6 Model fitting for stress relaxation. (a) The stress relaxation master curve at 16 °C. (b) The shifting factors with temperature.

($E(\infty)$) and E_1 = 1480 MPa ($E(0) - E_0$). By considering the volume fraction and the stress concentration factor of the matrix, the Young's modulus of the nonequilibrium branch is $E_{non} = E_1/(\gamma_M \nu_M)$ and therefore E_{non} = 3150 MPa. Using eqn (17) to fit the stress relaxation master curve at 16 °C, parameters τ_0 and β are determined as 110 s and 0.3, respectively. As introduced in Section 3, the shifting factors as functions of temperature can be described by WLF and Arrhenius equations at different temperature ranges. By fitting shifting factors with these two equations (Fig. 6b), parameters in eqn (7) and (8) are determined as C_1 = 24, C_2 = 50 °C, T_r = 16 °C and AF_c/k = −35 000 K.

4.2 Comparison between model simulations and experiments

Using parameters in Table 1, the model successfully predicts the triple-shape memory behavior under three different nominal stress pairs (P_1 = 0.1 MPa, P_2 = 0.3 MPa; P_1 = 0.15 MPa, P_2 = 0.45 MPa; P_1 = 0.2 MPa, P_2 = 0.6 MPa) (Fig. 7). It should be noted that these curves were not used for parameter identification. In Fig. 7, the model predictions show good agreement with experiments. The largest discrepancy occurs in S4 unloading to achieve the first temporary shape and in S8 heating back to ~40 °C to recover to the first temporary shape. Compared to the first temporary shape fixed in the experiments, a less temporary shape is fixed in predictions. We attribute this error primarily to the nonlinear deformation for the TSPC at 40 °C (Fig. 5b), which the neo-Hookean model for PCL crystals is unable to satisfactorily represent. At S8, the predictions reach the first temporary shape earlier than experiments, which is caused by the faster relaxation modulus in the model fitting (Fig. 6a).

The model also predicted the one-step-fixing shape memory behavior introduced in Section 2.4 with the 0.2 MPa imposed stress case (Fig. 8). Briefly, following high temperature deformation, then direct cooling to 0 °C and subsequent unloading, almost 100% strain was fixed. During continuous heating, recovery is interrupted as the strain reaches a plateau between T_g^{epoxy} and T_m^{PCL}, and then completes as T_m^{PCL} is surpassed. In Fig. 8, the model prediction shows good agreement with the experiment, indicating that the essential physics are captured.

4.3 Stress and strain energy analyses for the triple-shape memory behavior

In order to better understand the mechanism of fixing temporary shapes, stress and strain energy analyses for the t-SME under the 0.15–0.45 MPa stress pair were investigated. Fig. 9a provides the thermomechanical loading history. Fig. 9b shows the variation of the strain as a function of time. In Fig. 9c and e, the total stress is divided into the stress acting on the matrix and the stress acting on the fiber network. At S1, all stress comes from the matrix since the fiber network (PCL) is in the melt state. In addition, because the matrix is in its rubbery state, the stress on the matrix mainly comes from the equilibrium branch; the stress on the nonequilibrium branch is almost zero due to the large viscous strain developed, indicating that the

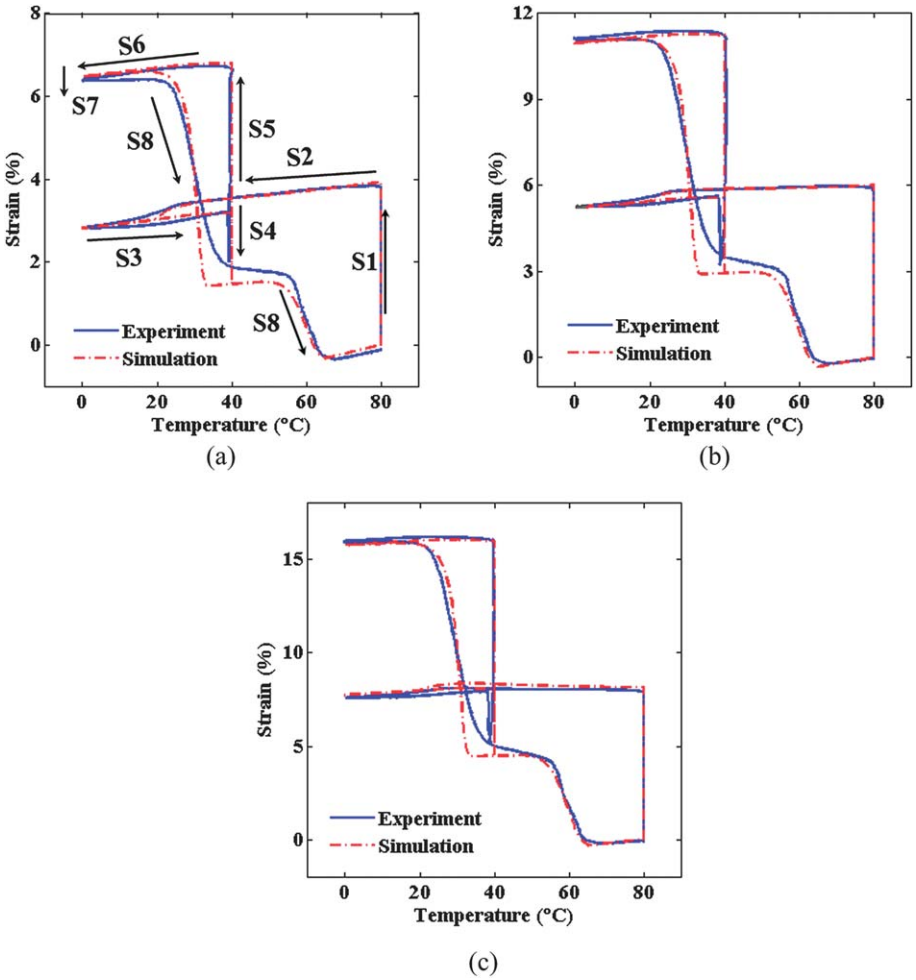

Fig. 7 Model predictions for triple shape memory behaviors under three different nominal stress pairs. (a) $P_1 = 0.1$ MPa, $P_2 = 0.3$ MPa. (b) $P_1 = 0.15$ MPa, $P_2 = 0.45$ MPa. (c) $P_1 = 0.2$ MPa, $P_2 = 0.6$ MPa.

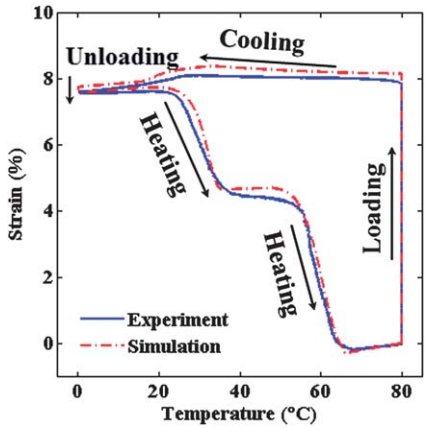

Fig. 8 Comparisons between model prediction and experimental result for the one-step-fixing shape memory behavior.

nonequilibrium branch is active for the subsequent shape memory effect. At S2 and S3, although crystals in the fiber network formed gradually, stress contribution from the fiber network is negligible due to small deformations on fiber crystals. At S4, after a quick unloading, the strain contracts ~50% (in S4 in Fig. 9b), which leads to a decrease of stress on the equilibrium branch of the matrix and the introduction of a compressive stress on the fiber network. Thus, the overall force balance is achieved and the total stress is zero. It is clear that the compressive stress on the fiber network prevents the matrix from returning to its stress-free (or initial) state. At S5 (the second loading), stresses on the matrix and the fiber network increase. At S6 (second cooling with holding a constant stress), stresses on the matrix and the fiber network stay constant. At S7 (unloading), stresses on the fiber network and on the equilibrium branch decrease slightly, but the stress on the nonequilibrium branch of the matrix changes quickly to a negative value, thus to prevent the material from recovery and maintain the force balance. At S8, during heating, viscosity on the nonequilibrium branch decreases, causing the decrease of the compressive stress on this branch. When the stress on the nonequilibrium branch decreases to zero, the material recovers to the first temporary shape and the stresses on the equilibrium branch and the fiber network return to the same values in S4. As the temperature is further increased to above the melting temperature, the stress on the fiber network starts to decrease;

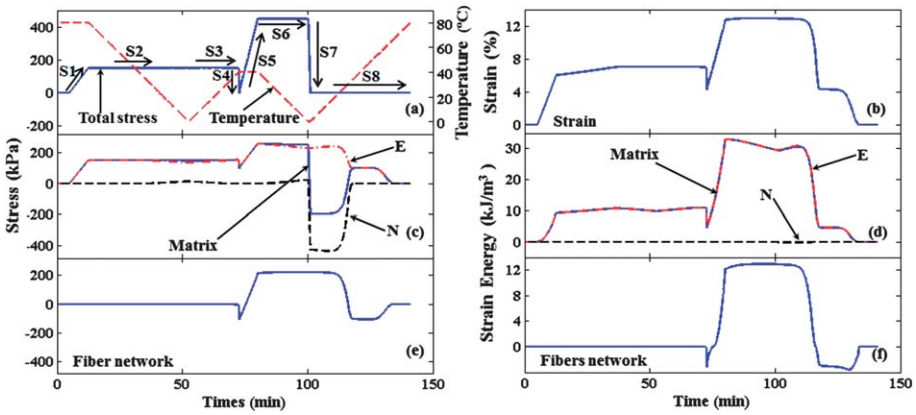

Fig. 9 Stress and strain analyses for the triple-shape memory behavior: (a) the thermomechanical loading history (stress and temperature *vs.* time). (b) Experimental output (strain). The total stress can be divided into the stress on the matrix (c) and the stress on the fiber network (e). The stress on the matrix (c) can be further divided into the one on the equilibrium branch ("E") and the one on the nonequilibrium branch ("N"). (d) The strain energy on the matrix, which can be divided into the one on the equilibrium branch ("E") and the one on the nonequilibrium branch ("N"). (f) The strain energy on the fiber network. In (d) and (f), the strain energy is taken as negative if the deformation is compressive.

when fiber crystals completely melt, the material recovers to its initial shape.

Fig. 9d and f show the variation of strain energy in the material. Comparing Fig. 9d and f, in S1, S2 and S3, the strain energy on the fiber network is nearly zero and most strain energy is from the equilibrium branch of the matrix. After the first unloading in S4, the strain energy on the equilibrium branch of the matrix drops and the strain energy on the fiber network is instantaneously generated to a negative value (due to compression). The energy release from the matrix is stored in the fiber crystals and a strain energy loss of $\sim$3 kJ m^{-3} (corresponding to a 30% loss) is observed. At S5 (loading at 40 °C), the strain energies on both the matrix and the fiber network increase. At S6 (cooling to 0 °C), the strain energy on the matrix decreases slightly, but that on the fiber network remains nearly constant. Upon unloading in S7, the strain energies on the equilibrium branch and the fiber network change slightly by transferring the energy to the nonequilibrium branch in the form of compressive energy ($-$0.2 kJ m^{-3}). During heating in S8, the strain energies stored on both the fiber network and the matrix decreases, and the strain energy on the nonequilibrium branch returns to zero when the material returns to the first temporary shape. Further heating the material to above its melting temperature, the energies stored on the fiber network and equilibrium branch decrease to zero and the material recovers to its permanent shape. It is also noted that since fiber crystals have a higher modulus than the equilibrium branch, the energy stored in the second temporary shape is much higher than that stored in the first temporary shape. For the material studied here, the energy stored in the second temporary shape is 42.6 kJ m^{-3}, which is 430% higher than that in the first temporary shape (8 kJ m^{-3}).

4.4 Stress and strain energy analyses for the one-step-fixing shape memory behavior

Similarly to the triple-shape memory behavior, stress and strain energy analyses were investigated for the one-step-fixing shape memory behavior. Fig. 10a provides the thermomechanical

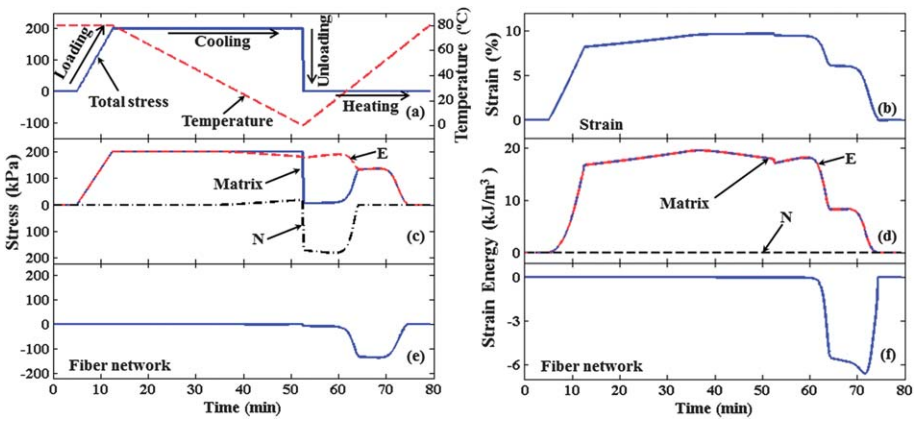

Fig. 10 Stress and strain analyses for the one-step-fixing shape memory behavior: (a) the thermomechanical loading history (stress and temperature *vs.* time). (b) Experimental output (strain). The total stress can be divided into the stress on the matrix (c) and the stress on fiber networks (e). The stress on the matrix (c) can be divided into the one on the equilibrium branch ("E") and the one on the nonequilibrium branch ("N"). (d) The strain energy on the matrix, which can be divided into the one on the equilibrium branch ("E") and the one on the nonequilibrium branch ("N"). (f) The strain energy on the fiber networks.

loading history. Fig. 10b shows the variation of the strain as a function of time. In Fig. 10c and e, the total stress is divided into the stress acting on the matrix and the stress acting on the fiber network. During the loading step, all stress comes from the matrix since the fiber network (PCL) is in the melt state. In addition, because the matrix is in its rubbery state, the stress on the matrix mainly comes from the equilibrium branch; the stress in the nonequilibrium branch is almost zero due to the large viscous strain developed, indicating that the nonequilibrium branch is active for the subsequent shape memory effect. In the cooling step, although crystals in the fiber network formed gradually, stress contribution from the fiber network is negligible due to small deformations on the fiber network. During unloading, stresses on the fiber network and on the equilibrium branch decrease slightly, but the stress on the nonequilibrium branch of the matrix changes quickly to a negative value, thus to prevent the material from recovery and maintain the force balance. During heating from 0 °C to ~40 °C, the viscosity on the nonequilibrium branch decreases, causing the decrease of the compressive stress on this branch. When the stress on the nonequilibrium branch decreases to zero, the material arrives at a strain plateau from ~40 °C to 60 °C (Fig. 10b) and the compressive stress on the fiber network maintains the force balance, which indicates that part of the strain is fixed by compressing the fiber crystals. As the temperature is further increased to exceed the melting temperature, the stress on the fiber network starts to decrease; when fiber crystals completely melt, the material recovers to its initial shape.

5 Conclusion

Triple-shape memory behaviors of TSPC were investigated in this paper. A 1D model was presented to describe the tripe-shape memory behaviors. The model separately considers the glass transition and melt–crystal transition. This separate treatment allows the material parameters used in the model to be independently identified from experiments. With parameters identified from stress relaxation tests and uniaxial isothermal tension tests, the model is able to predict the triple-shape memory behaviors and the one-step-fixing shape memory behavior. The stress and strain energy analyses from the model revealed clearly the shape fixing mechanisms for TSPC. For the triple-shape memory behavior, the first temporary shape is fixed by fiber crystals and the second temporary shape is fixed by the nonequilibrium branch. For the one-step-fixing shape memory behavior, the temporary shape is firstly fixed by the nonequilibrium branch at low temperature as the matrix is in the glassy state. During heating, when the matrix transfers gradually from the glassy state to the rubbery state, the fiber network becomes deformed to fix a part of the temporary shape, which gives way to complete recovery upon further heating.

Acknowledgements

We gratefully acknowledge the support of an NSF CAREER award (CMMI-0645219), and an AFOSR grant (FA9550-09-1-0195; Dr B.-L. "Les" Lee, Program Manager).

References

1 A. Lendlein and S. Kelch, Shape-memory polymers, *Angew. Chem., Int. Ed.*, 2002, **41**, 2035–2057.
2 A. Lendlein and S. Kelch, Shape-memory polymers as stimuli-sensitive implant materials, *Clin. Hemorheol. Microcirc.*, 2005, **32**, 105–116.
3 C. Liu, H. Qin and P. T. Mather, Review of progress in shape-memory polymers, *J. Mater. Chem.*, 2007, **17**, 1543–1558.
4 P. T. Mather, X. F. Luo and I. A. Rousseau, Shape memory polymer research, *Annu. Rev. Mater. Res.*, 2009, **39**, 445–471.
5 T. Xie, Recent advances in polymer shape memory, *Polymer*, 2011, **52**, 4985–5000.
6 H. Y. Jiang, S. Kelch and A. Lendlein, Polymers move in response to light, *Adv. Mater.*, 2006, **18**, 1471–1475.
7 H. Koerner, G. Price, N. A. Pearce, M. Alexander and R. A. Vaia, Remotely actuated polymer nanocomposites – stress-recovery of carbon-nanotube-filled thermoplastic elastomers, *Nat. Mater.*, 2004, **3**, 115–120.
8 A. Lendlein, H. Y. Jiang, O. Junger and R. Langer, Light-induced shape-memory polymers, *Nature*, 2005, **434**, 879–882.
9 M. H. Li, P. Keller, B. Li, X. G. Wang and M. Brunet, Light-driven side-on nematic elastomer actuators, *Adv. Mater.*, 2003, **15**, 569–572.
10 T. F. Scott, R. B. Draughon and C. N. Bowman, Actuation in crosslinked polymers *via* photoinduced stress relaxation, *Adv. Mater.*, 2006, **18**, 2128–2132.
11 T. F. Scott, A. D. Schneider, W. D. Cook and C. N. Bowman, Photoinduced plasticity in cross-linked polymers, *Science*, 2005, **308**, 1615–1617.
12 K. N. Long, T. F. Scott, M. L. Dunn and H. J. Qi, Photo-induced deformation of active polymer films: single spot irradiation, *Int. J. Solids Struct.*, 2011, **48**, 2089–2101.
13 K. N. Long, T. F. Scott, H. J. Qi, C. N. Bowman and M. L. Dunn, Photomechanics of light-activated polymers, *J. Mech. Phys. Solids*, 2009, **57**, 1103–1121.
14 K. N. Long, M. L. Dunn, T. F. Scott, L. P. Turpin and H. J. Qi, Light-induced stress relief to improve flaw tolerance in network polymers, *J. Appl. Phys.*, 2010, **107**, 053519.
15 W. M. Huang, B. Yang, L. An, C. Li and Y. S. Chan, Water-driven programmable polyurethane shape memory polymer: demonstration and mechanism, *Appl. Phys. Lett.*, 2005, **86**, 114105.
16 R. Mohr, K. Kratz, T. Weigel, M. Lucka-Gabor, M. Moneke and A. Lendlein, Initiation of shape-memory effect by inductive heating of magnetic nanoparticles in thermoplastic polymers, *Proc. Natl. Acad. Sci. U. S. A.*, 2006, **103**, 3540–3545.
17 C. M. Yakacki, R. Shandas, C. Lanning, B. Rech, A. Eckstein and K. Gall, Unconstrained recovery characterization of shape-memory polymer networks for cardiovascular applications, *Biomaterials*, 2007, **28**, 2255–2263.
18 Y. P. Liu, K. Gall, M. L. Dunn, A. R. Greenberg and J. Diani, Thermomechanics of shape memory polymers: uniaxial experiments and constitutive modeling, *Int. J. Plast.*, 2006, **22**, 279–313.

19 Y. P. Liu, K. Gall, M. L. Dunn and P. McCluskey, Thermomechanics of shape memory polymer nanocomposites, *Mech. Mater.*, 2004, **36**, 929–940.
20 H. Tobushi, H. Hara, E. Yamada and S. Hayashi, Thermomechanical properties in a thin film of shape memory polymer of polyurethane series, *Smart Mater. Struct.*, 1996, **5**, 483–491.
21 Z. Wang, C. Hansen, Q. Ge, S. H. Maruf, D. U. Ahn, H. J. Qi and Y. F. Ding, Programmable, pattern-memorizing polymer surface, *Adv. Mater.*, 2011, **23**, 3669–3673.
22 J. Ryu, M. D'Amato, X. D. Cui, K. N. Long, H. J. Qi and M. L. Dunn, Photo-origami-Bending and folding polymers with light, *Appl. Phys. Lett.*, 2012, **100**, 161908.
23 H. J. Qi, T. D. Nguyen, F. Castro, C. M. Yakacki and R. Shandas, Finite deformation thermo-mechanical behavior of thermally induced shape memory polymers, *J. Mech. Phys. Solids*, 2008, **56**, 1730–1751.
24 T. D. Nguyen, H. J. Qi, F. Castro and K. N. Long, A thermoviscoelastic model for amorphous shape memory polymers: incorporating structural and stress relaxation, *J. Mech. Phys. Solids*, 2008, **56**, 2792–2814.
25 F. Castro, K. K. Westbrook, K. N. Long, R. Shandas and H. J. Qi, Effects of thermal rates on the thermomechanical behaviors of amorphous shape memory polymers, *Mech. Time-Depend. Mater.*, 2010, **14**, 219–241.
26 Q. Ge, K. Yu, Y. F. Ding and H. J. Qi, Prediction of temperature-dependent free recovery behaviors of amorphous shape memory polymers, *Soft Matter*, 2012, **8**, 11098–11105.
27 X. F. Luo and P. T. Mather, Preparation and characterization of shape memory elastomeric composites, *Macromolecules*, 2009, **42**, 7251–7253.
28 Q. Ge, X. F. Luo, E. D. Rodriguez, X. Zhang, P. T. Mather, M. L. Dunn and H. J. Qi, Thermomechanical behavior of shape memory elastomeric composites, *J. Mech. Phys. Solids*, 2012, **60**, 67–83.
29 K. N. Long, M. L. Dunn and H. J. Qi, Mechanics of soft active materials with phase evolution, *Int. J. Plast.*, 2010, **26**, 603–616.
30 K. K. Westbrook, V. Parakh, T. Chung, P. T. Mather, L. C. Wan, M. L. Dunn and H. J. Qi, Constitutive modeling of shape memory effects in semicrystalline polymers with stretch induced crystallization, *J. Eng. Mater. Technol.*, 2010, **132**, 041010.
31 T. Xie, Tunable polymer multi-shape memory effect, *Nature*, 2010, **464**, 267–270.
32 K. Yu, T. Xie, J. S. Leng, Y. F. Ding and H. J. Qi, Mechanisms of multi-shape memory effects and associated energy release in shape memory polymers, *Soft Matter*, 2012, **8**, 5687–5695.
33 I. Bellin, S. Kelch, R. Langer and A. Lendlein, Polymeric triple-shape materials, *Proc. Natl. Acad. Sci. U. S. A.*, 2006, **103**, 18043–18047.
34 I. Bellin, S. Kelch and A. Lendlein, Dual-shape properties of triple-shape polymer networks with crystallizable network segments and grafted side chains, *J. Mater. Chem.*, 2007, **17**, 2885–2891.
35 X. F. Luo and P. T. Mather, Triple-shape polymeric composites (TSPCs), *Adv. Funct. Mater.*, 2010, **20**, 2649–2656.
36 T. Xie, X. C. Xiao and Y. T. Cheng, Revealing triple-shape memory effect by polymer bilayers, *Macromol. Rapid Commun.*, 2009, **30**, 1823–1827.
37 H. Tobushi, S. Hayashi, A. Ikai and H. Hara, Thermomechanical properties of shape memory polymers of polyurethane series and their applications, *J. Phys. IV*, 1996, **6**, 377–384.
38 F. Castro, K. K. Westbrook, J. Hermiller, D. U. Ahn, Y. F. Ding and H. J. Qi, Time and temperature dependent recovery of epoxy-based shape memory polymers, *J. Eng. Mater. Technol.*, 2011, **133**, 021025.
39 Y. C. Chen and D. C. Lagoudas, A constitutive theory for shape memory polymers. Part I-Large deformations, *J. Mech. Phys. Solids*, 2008, **56**, 1752–1765.
40 Y. C. Chen and D. C. Lagoudas, A constitutive theory for shape memory polymers. Part II-A linearized model for small deformations, *J. Mech. Phys. Solids*, 2008, **56**, 1766–1778.
41 K. K. Westbrook, P. H. Kao, F. Castro, Y. F. Ding and H. J. Qi, A 3D finite deformation constitutive model for amorphous shape memory polymers: a multi-branch modeling approach for nonequilibrium relaxation processes, *Mech. Mater.*, 2011, **43**, 853–869.
42 G. Barot and I. J. Rao, Constitutive modeling of the mechanics associated with crystallizable shape memory polymers, *Z. Angew. Math. Phys.*, 2006, **57**, 652–681.
43 H. F. Brinson, *Polymer Engineering Science and Viscoelasticity: An Introduction*, Springer, New York, 2007.
44 M. Rubinstein and R. H. Colby, *Polymer Physics*, Oxford University Press, Oxford; New York, 2003.
45 Y. Benveniste, A new approach to the application of Mori-Tanaka theory in composite-materials, *Mech. Mater.*, 1987, **6**, 147–157.
46 P. P. Castaneda, The effective mechanical-properties of nonlinear isotropic composites, *J. Mech. Phys. Solids*, 1991, **39**, 45–71.
47 M. L. Dunn, One-dimensioal composite micromechanics, *Int. J. Mech. Eng. Educ.*, 1997, **26**, 38–50.
48 G. Williams and D. C. Watts, Non-symmetrical dielectric relaxation behaviour arising from a simple empirical decay function, *Trans. Faraday Soc.*, 1970, **66**, 80–85.
49 P. A. O'Connell and G. B. McKenna, Arrhenius-type temperature dependence of the segmental relaxation below T_g, *J. Chem. Phys.*, 1999, **110**, 11054–11060.
50 M. L. Williams, R. F. Landel and J. D. Ferry, Temperature dependence of relaxation mechanisms in amorphous polymers and other glass-forming liquids, *Phys. Rev.*, 1955, **98**, 1549.
51 E. A. Di Marzio and A. J. M. Yang, Configurational entropy approach to the kinetics of glasses, *J. Res. Natl. Inst. Stand. Technol.*, 1997, **102**, 135–157.
52 K. R. Rajagopal and A. R. Srinivasa, Mechanics of the inelastic behavior of materials – part 1, theoretical underpinnings, *Int. J. Plast.*, 1998, **14**, 945–967.

53 K. R. Rajagopal and A. R. Srinivasa, Mechanics of the inelastic behavior of materials. Part II: inelastic response, *Int. J. Plast.*, 1998, **14**, 969–995.
54 M. Negahban and A. S. Wineman, Modeling the mechanical response of a material undergoing continuous isothermal crystallization, *Int. J. Eng. Sci.*, 1992, **30**, 953–962.
55 M. Negahban, Simulation of mechanical response in crystallizing polymers – crystallization under constant shearing deformations, *Mech. Mater.*, 1993, **16**, 379–399.
56 R. Ma and M. Negahban, Simulation of mechanical response in crystallizing polymers – crystallization under a constant shear force, *Acta. Mech.*, 1995, **112**, 59–76.
57 R. J. Ma and M. Negahban, Simulation of mechanical response during polymer crystallization around rigid inclusions and voids – homogeneous crystallization, *Mech. Mater.*, 1995, **21**, 25–50.
58 A. V. Tobolsky, *Properties and Structures of Polymers*, Wiley, New York, 1960.
59 A. Wineman and J. H. Min, Time dependent scission and cross-linking in an elastomeric cylinder undergoing circular shear and heat conduction, *Int. J. Non Lin. Mech.*, 2003, **38**, 969–983.
60 A. Wineman, Some comments on the mechanical response of elastomers undergoing scission and healing at elevated temperatures, *Math. Mech. Solid.*, 2005, **10**, 673–689.
61 A. Wineman and J. Shaw, Influence of thermally induced scission and crosslinking on the post-scission inflation of circular elastomeric membranes, *Int. J. Eng. Sci.*, 2008, **46**, 758–774.
62 G. Barot, I. J. Rao and K. R. Rajagopal, A thermodynamic framework for the modeling of crystallizable shape memory polymers, *Int. J. Eng. Sci.*, 2008, **46**, 325–351.
63 H. J. Qi, T. D. Nguyen, F. Castro, C. M. Yakacki and R. Shandas, Finitede formation thermo-mechanical behavior of thermally induced shape memory polymers, *J. Mech. Phys. Solids*, 2008, **56**, 1730–1751.
64 M. Avrami, Kinetics of phase change I – general theory, *J. Chem. Phys.*, 1939, **7**, 1103–1112.
65 M. Avrami, Kinetics of phase change II – transformation-time relations for random distribution of nuclei, *J. Chem. Phys.*, 1940, **8**, 212–224.
66 M. Avrami, Granulation, phase change, and microstructure – kinetics of phase change. III, *J. Chem. Phys.*, 1941, **9**, 177–184.